RSC Advances

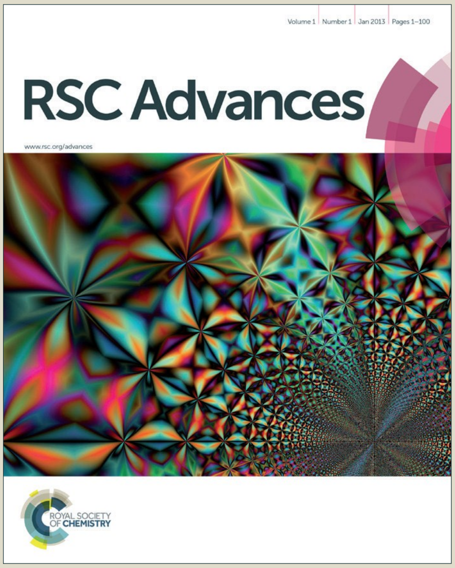

ROYAL SOCIETY OF CHEMISTRY

www.rsc.org/advances

The New Dicyanoruthenium(III) Building Block with 2'-Hydroxyacetophenone Imine for Heterobimetallic Complexes

Jing Ru,[a] Tian-Xiang Zong,[a] Jing-Yuan Ge,[a] Min-Xia Yao,[b] and Jing-Lin Zuo*[a]

[a]*State Key Laboratory of Coordination Chemistry, School of Chemistry and Chemical Engineering, Collaborative Innovation Center of Advanced Microstructures, Nanjing University, Nanjing 210093, P. R. China*

[b]*School of Science, Nanjing University of Technology, Nanjing 210009, P. R. China*

ABSTRACT: A new ruthenium(III)-based building block, *trans*-(Ph_4P)[$Ru^{III}(L)_2(CN)_2$] (L = 2'-hydroxyacetophenone imine), has been synthesized and characterized. Reactions of this building block with different Mn^{III} Schiff base (SB) complexes, [$Mn(SB)(H_2O)_2$]ClO_4, result in the 1-D zigzag chain complexes, [$Ru^{III}(L)_2(CN)_2Mn^{III}(SB)$]$_n$ (SB = salen, **1**; salcy, **2**; nappa, **4**; napcy, **5**), respectively. X-ray crystallographic studies reveal that each of Mn^{III} centers has a distorted octahedral environment, while complex **3** possesses a single cationic chain structure consisting of [$Cu(chxn)_2$][$Ru(L)_2(CN)_2$]$_n$ units and their corresponding [$Ru(L)_2(CN)_2$]$^-$ anions. Compounds **1**–**3** exhibit antiferromagnetic coupling between the Ru^{III} and Mn^{III}/Cu^{II} centers, whereas **4** and **5** reveal ferromagnetic coupling between the Ru^{III} and Mn^{III} centers through the cyano bridges. Furthermore, magneto-structural correlation for some typical cyano-bridged heterobimetallic Ru^{III}–Mn^{III}/Cu^{II} compounds is discussed.

Abbreviations: salen = *N,N'*-ethylenebis(salicylideneimine) dianion, salcy = *N,N'*-(1,2-cyclohexanediylethylene)bis(salicylideneiminato) dianion, chxn = 1,2-Diaminocyclohexane, nappa = *N,N'*-(1-methylethylene) bis(2-

---

* To whom correspondence should be addressed. Email: zuojl@nju.edu.cn; Fax: +86-25-83314502.
Nanjing University.

hydroxynaphthalene-1-carbaldehydene-iminate) dianion, napcy = *N,N'*-(1,2-cyclohexanediylethylene)bis(2-hydroxynaphthalene-1carbaldehydene-iminate) dianion.

Introduction

Low-dimensional magnetic materials, such as single-molecule magnets (SMMs) and single-chain magnets (SCMs) with slow magnetic relaxation, have been extensively studied due to their unique potential applications for molecular devices, high-density information storage, and quantum computers.[1]

Recently, more and more molecule-based magnets based on 4d and 5d metal ions have been reported.[2] An essential driving force for the interest in this area is because the heavier metal ions can contribute significantly to the physical properties of paramagnetic compounds. More specifically, the heavier metals possess more diffuse valent orbitals than 3d metals, which can result in stronger magnetic exchange interactions.[3] The 4d/5d metal ions are characterized by large spin-orbit coupling that is instrumental in magnetic anisotropy.[4,5] In the synthesis of paramagnetic materials, most efforts have been devoted to cyanide precursors, especially to those of Nb,[6] Mo,[7] W,[8] and Re[9] compounds, whereas low-dimensional magnetic materials incorporating Ru and Os units received less attention. With regard to the Ru(III)-containing building blocks, such like *trans*-$[Ru^{III}(L_1)_2(CN)_2]^-$ (L_1= 8-quinolinolato (Q) and acetylacetone anion (acac))[10] and *trans*-$[Ru^{III}(salen)(CN)_2]^-$ (H_2salen = *N,N'*-bis(salicylidene)ethylenediamine) [11], they are used to construct a series of Ru^{III}–3d and Ru^{III}–4f polynuclear complexes that exhibit a variety of novel structural and magnetic properties. Recently, a new heteroleptic cyanido-Schiff base complex $[K(H_2O)_2Ru^{III}(valen)(CN)_2]\cdot H_2O$ as a building block and its corresponding Ru^{III}–4f heterometallic complexes with one-dimensional structures have been reported.[12]

Given the above mentioned *trans*-dicyano Ru complexes as useful building blocks, low-dimensional magnetic materials are easily constructed via the cyano bridges.[13] For example, when building blocks of ((*R*,*R*) or (*S*,*S*))-$[Bu_4N][Ru(5\text{-}Cl\text{-}salcy)](CN)_2]$ (salcy = *N,N'*-(1,2-cyclohexanediylethylene)bis(salicylideneiminato)dianion) and

$[Ru(salen)(CN)_2]^-$ are employed, a series of cyano-bridged chains and clusters that behave as ferrimagnets, SCMs, or metamagnets have been investigated in our previous work.[14] And the design of novel cyanoruthenium(III) building blocks continues to be intriguing to us. Phenolic oxime ligands are extensively studied in extractive hydrometallurgy,[15] however, the cooperative electronic properties in materials formed by transition metal complexes with cyanide ligands have been overlooked to date.

Herein, a new dicyanoruthenium(III) complex incorporating a relevant phenolic oxime, 2-Hydroxyethanoneoxime, is reported. During the reaction, the oxime is reduced to imine by $Ru(PPh_3)_3Cl_2$[16] and thus leading to the formation of complex $PPh_4[Ru(L)_2(CN)_2]$ (L=2'-hydroxyacetophenone imine). Based on the Ru-containing building block and its relevant hetorometallic units, five cyano-connected heterobimetallic one-dimensional (1D) chain complexes, $[Ru(L)_2(CN)_2Mn(salen)]_n$ (**1**), $[Ru(L)_2(CN)_2Mn(salcy)]_n$ (**2**), $[Ru(L)_2(CN)_2Cu(chxn)]_n$ (**3**), $[Ru(L)_2(CN)_2Mn(nappa)]_n$ (**4**), and $[Ru(L)_2(CN)_2Mn(napcy)]_n$ (**5**), have been synthesized and fully studied. In addition, magneto-structural correlation for some typical cyano-bridged heterobimetallic Ru^{III}–Mn^{III}/Cu^{II} compounds is accordingly discussed.

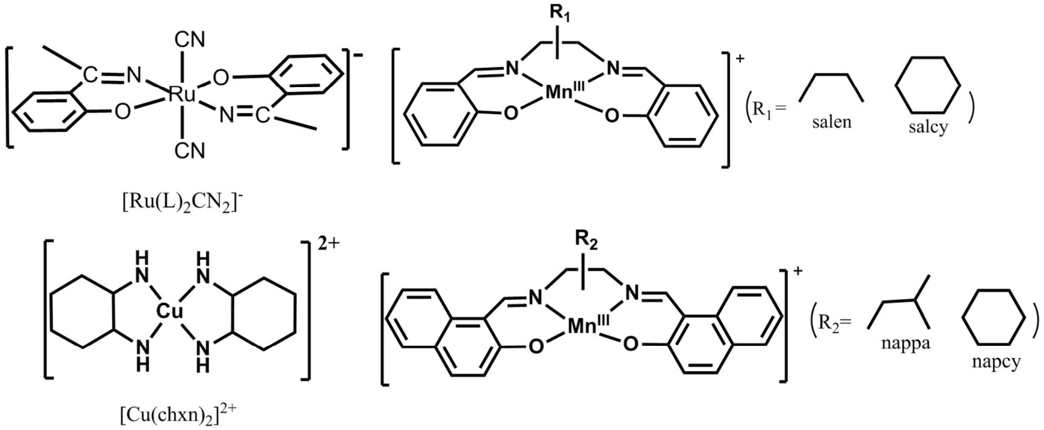

Scheme 1

Experimental Section

General Methods. All reagents and solvents were commercially available and used as received without further purification. [Mn(salen)(H_2O)$_2$]ClO_4,[17] [Mn(salcy)(H_2O)$_2$]ClO_4,[17] [Mn(nappa)(H_2O)$_2$]ClO_4,[17] [Mn(napcy)(H_2O)$_2$]ClO_4,[17] [Cu(chxn)$_2$(H_2O)$_2$](NO_3)$_2$,[18] Me-saoH_2 and Ru(L)(PPh_3)Cl were prepared according to previously reported methods.[16] (Ph_4P)[Ru(L)$_2$(CN)$_2$] was carried out by a procedure similar to that for (Bu_4N)[Ru(salen)(CN)$_2$] with minor modifications.[19]

(Ph_4P)[Ru(L)$_2$(CN)$_2$]: Ru(L)PPh_3Cl (1.33 g, 2.00 mmol) was refluxed with NaCN (25.0 mg, 5.00 mmol) in 50 mL of methanol for 1 h. The solution was evaporated to dryness and the residue then dissolved in 10 mL of water. Addition of Ph_4PCl (556 mg, 2.00 mmol) to the aqueous solution produced a purple precipitate which was collected, washed with water, and dried in vacuo. Yield: 48%. Anal. Calcd for $C_{38}H_{54}N_5O_2Cl_2Ru$: C, 58.15; H, 6.93; N, 8.92. Found: C, 58.32; H, 6.71; N, 8.79. ESI-MS: (*m/z*) 544 (M^-). Selected IR data (KBr, cm^{-1}): 2096 (ν(C≡N)).

Preparation of [Ru(L)$_2$(CN)$_2$Mn(salen)]$_n$ (1): A solution of [Mn(salen)(H_2O)$_2$]]ClO_4 (18.2 mg, 40.0 μmol) in 10 mL of methanol was added to a solution of (Ph_4P) [Ru(L)$_2$(CN)$_2$] (35.6 mg, 40.0 μmol) in 10 mL of acetonitrile. After stirring for 10 min, the resulted dark-brown solution was filtered off and then left undisturbed. The slow evaporation of the filtrate at room temperature gave dark-brown rod-like crystals of **1** after two weeks. Yield: 54%. Anal. Calcd for $C_{68}H_{56}Mn_2N_{12}O_8Ru_2$: C, 55.14; H, 3.81; N, 11.35. Found: C, 55.36; H, 3.57; N, 11.01. Selected IR data (KBr, cm^{-1}): 2106 (ν(C≡N)).

Preparation of [Ru(L)$_2$(CN)$_2$Mn(salcy)]$_n$ (2). Preparation was similar to that of **1** by using [Mn(salcy)(H_2O)$_2$]ClO_4 (20.4 mg, 40.0 μmol) instead of [Mn(salen)(H_2O)$_2$]]ClO_4. The slow evaporation of the filtrate resulted in dark-green needles of **2** after two weeks. Yield: 60%. Anal. Calcd for $C_{38}H_{32}MnN_6O_4Ru$: C, 57.58; H, 4.07; N, 10.60. Found: C, 57.35; H, 4.28; N, 10.85. Selected IR data (KBr, cm^{-1}): 2113 (ν(C≡N)).

Preparation of [Ru(L)$_2$(CN)$_2$Cu(chxn)]$_n$ (3). Preparation was similar to that of **1** by using Cu(chxn)$_2$(NO_3)$_2$ (16.8 mg, 40.0 μmol) instead of [Mn(salen)(H_2O)$_2$]]ClO_4. The slow evaporation of the filtrate gave dark-green needles of **3** after two weeks. Yield:

60%. Anal. Calcd for $C_{48}H_{44}CuN_{12}O_4Ru_2$: C, 51.54; H, 3.96; N, 15.03. Found: C, 51.27; H, 4.12; N, 15.22. Selected IR data (KBr, cm^{-1}): 2094 (ν(C≡N)).

Preparation of [Ru(L)$_2$(CN)$_2$Mn(nappa)]$_n$ (4). Complex **4** was obtained as black block crystals by slow diffusion of a methanol solution (5 mL) of $(Ph_4P)[Ru(L)_2(CN)_2]$ (35.6 mg, 40.0 μmol) and an acetonitrile solution (5 mL) of $[Mn(nappa)(H_2O)_2]ClO_4$ (22.8 mg, 40.0 μmol) through an H-shaped tube at room temperature for about one month. The resulting crystals were collected, washed with methanol, and dried in air. Yield: 52%. Anal. Calcd for $C_{43}H_{34}MnN_6O_4Ru$: C, 60.42; H, 4.01; N, 9.83. Found: C, 60.13; H, 4.25; N, 10.01. Selected IR data (KBr, cm^{-1}): 2113 (ν(C≡N)).

Preparation of [Ru(L)$_2$(CN)$_2$Mn(napcy)]$_n$ (5). Preparation was similar to that of **4**, with the exception of $[Mn(napcy)(H_2O)_2]ClO_4$ (24.4 mg, 40.0 μmol) used instead. The slow evaporation of the filtrate gave dark-green needles of **5** after one month. Yield: 55%. Anal. Calcd for $C_{46}H_{32}MnN_6O_4Ru$: C, 62.16; H, 3.63; N, 9.46. Found: C, 62.39; H, 3.81; N, 9.21. Selected IR data (KBr, cm^{-1}): 2114 (ν(C≡N)).

X-ray Structure Determination. The crystal structures were determined with a Siemens (Bruker) SMART CCD diffractometer using monochromated Mo Kα radiation (λ= 0.71073 Å). The cell parameters were retrieved using SMART software and refined using SAINT[20] for all observed reflections. Data were collected using a narrow-frame method with scan widths of 0.30° in ω and an exposure time of 10 s/frame. The absorption corrections were applied using SADABS[21] supplied by Bruker. Structures were solved by direct methods using the SHELXL program.[22] The positions of metal atoms and their first coordination spheres were located from direct methods E-maps. The other non-hydrogen atoms were found in alternating difference Fourier syntheses and least-squares refinement cycles and, during the final cycles, refined anisotropically. Hydrogen atoms were placed in calculated positions and refined as riding atoms with a uniform value of U_{iso}. Final crystallographic data and values of R_1 and wR_2 are listed in Table 1. Selected bond distances and angles for complexes **1**−**5** are listed in Tables 2–6.† CCDC reference numbers are 1400054 (**1**), 1400055 (**2**), 1400056 (**3**), 1400057 (**4**), and 1400058 (**5**), respectively.

Physical Measurements. Elemental analyses for C, H, and N were performed on a Perkin-Elmer 240C analyzer. Infrared spectra were recorded on a Vector22 Bruker Spectrophotometer with KBr pellets in the 400−4000 cm^{-1} region. Magnetic susceptibilities for polycrystalline samples were measured with the use of a Quantum Design MPMS-SQUID-VSM magnetometer in the temperature range of 1.9–300 K. Field dependences of magnetization were measured using Quantum Design MPMS-SQUID-VSM system in an applied field up to 70 kOe.

Results and discussion

Syntheses and Spectroscopic Studies

In this paper, $Na[Ru^{III}(L)_2(CN)_2]$ was synthesized from the reaction of $Ru(L)_2(PPh_3)Cl$ and NaCN. After the reaction with Ph_4PCl, the dicyanometalate precursor, $(PPh_4)[Ru^{III}(L)_2(CN)_2]$, was prepared in good yield. $(PPh_4)[Ru^{III}(L)_2(CN)_2]$ is soluble in most common organic solvents, such as methanol, acetonitrile, chloroform, and *N*,*N*-dimethylformamide. The C≡N stretching frequency is located at 2096 cm^{-1}, which is comparable to those reported in Ru(III) dicyanides, such as $(PPh_4)[Ru(Q)_2(CN)_2]$ (2095 cm^{-1}),[10] $Na[Ru^{III}(salen)(CN)_2]$ (2080 cm^{-1}),[19] and ((*R,R*) or (*S,S*))-$[Bu_4N][Ru(5\text{-Cl-Salcy})](CN)_2]$ (2096 cm^{-1}).[14]

The reactions of $(PPh_4)[Ru^{III}(L)_2(CN)_2]$ and its corresponding metallic counter parts $[Mn(SB)(H_2O)_2]^+$ or $[Cu(chxn)]^{2+}$ in methanol (or methanol/acetonitrile) lead to the formation of one-dimensional heterobimetallic complexes **1**−**5**. In IR spectra, C≡N stretching vibrations are observed (2106 cm^{-1} for **1**, 2113 cm^{-1} for **2**, 2096 cm^{-1} for **3**, 2113 cm^{-1} for **4**, and 2114 cm^{-1} for **5**), which is consistent with other Ru^{III}−M bimetallic compounds.[10a]

Structural Description

The structural parameters such as key bond lengths and angles are listed in Table 2. The crystal structures of complexes **1**−**5** are shown in Figures 1−5, respectively. With the use of different Schiff base ligands, complexes **1**, **2**, **4**, and **5** show similar structures, demonstrated by the crystal cell parameters listed in Table 1 that all crystals sit in the triclinic space group. The asymmetric unit of **1, 2, 4, and 5** is composed of one $[Mn^{III}(SB)]^+$ cation and two $[Ru(L)_2(CN)_2]^-$ anions. For the

$[Mn^{III}(SB)]^+$ cations, SB ligands adopt a quasi-planar chelating mode, resulting in the coordination to the Mn^{III} ion along the equatorial plane. Such coordination mode leaves the axial sites available to be trans-coordinated by N atoms from cyanide bridges， thus forming a 1-D $(-Ru-C\equiv N-Mn-N\equiv C-)_n$ liner chain. The axial $Mn-N_{cyanide}$ bond lengths (2.248(4)–2.396(5) Å) are significantly longer than the equatorial Mn−N(O) (1.883(4)–2.011(5) Å) lengths, forming the elongated octahedral configuration derived from Jahn-Teller distortion of Mn^{III}. The bond angles of Mn–$N–C_{cyanide}$ are: 158.2(5)–163.6(4)° for **1**, 150.1(5)–153.3(4)° for **2**, 171.9(3)–176.2(4)° for **4**, and 172.1(5)–172.9(7)° for **5**, respectively. With regard to the moiety of $[Ru(L)_2(CN)_2]^-$, the coordination environment of Ru^{III} can also be described as a distorted octahedron, consisting of two N atoms (salen ligand), two C atoms (cyanide groups), and two O atoms (phenolic oxygen). The average Ru−N(O) bond length is 2.015(4) Å, whereas the mean Ru−C length is 2.079(4) Å, whichtrend agrees well with other $Ru^{III}-M$ bimetallic compounds.[10a] The $Ru-C\equiv N$ angles (174.0(5)–178.4(3)°) show slight deviation from linearity. With respect to the molecular chains, complex **1**, for instance, is running along the *b* axis with the intrachain Ru···Mn separation of 5.457(3) Å through the bridging cyanide. The shortest interchain Ru···Ru, Mn···Mn, and Ru···Mn distances are 7.232, 6.732, and 8.099 Å, respectively, obviously longer than the intrachain metal···metal distances.

There is no significant interaction between two neighboring chains except for **4**. Each chain interacts with the two adjacent chains via π–π stacking between aromatic rings of the salcy ligands with a centroid distance of 3.353 Å, thus forming the 3D structure (Figure S1).

Treatment of $Cu(chxn)_2(NO_3)_2$ with *trans*-$(Ph_4P)[Ru(L)_2(CN)_2]$ in methanol at room temperature gives complex **3** (Figure 3). Complex **3** displays a single cationic chain structure consisting of a $[Cu(chxn)_2][Ru(L)_2(CN)_2]_n$ unit and a free $[Ru(L)_2(CN)_2]^-$ anion. The Cu^{II} center has a distorted octahedral environment coordinated by four equatorial nitrogen atoms from two chxn ligands and two axial nitrogen atoms from $[Ru(L)_2(CN)_2]^-$ units with a trans configuration. The $Cu-N_{cyanide}$ length of 2.411(4) Å is slightly longer than the $Cu-N_{chxn}$ lengths [2.002(4) and 2.051(3) Å]. The bridging $Ru-C\equiv N$ angle is 177.9(4)°. The bond lengths in each $[Ru(L)_2(CN)_2]^-$ unit [Ru–O of 1.982(3)–1.988(3)Å and Ru–N of 2.046(4)–2.048(3) Å] are similar to those found in *trans*-$(Ph_4P)[Ru(acac)_2(CN)_2]$.[10a] Furthermore, the intramolecular Cu···Ru distance is 4.981 Å, along with the Cu-N-C-Ru torsion angle of −160.2° and the closest intermolecular Ru···Ru separation of 6.012 Å.

Magnetic Properties

Magnetic susceptibility measurements were performed on polycrystalline samples of complexes **1**−**5** using the SQUID magnetometer at temperatures ranging from 1.9 K to 300 K.

Magnetic properties of 1 and 2. As shown in Figures 6 and **7**, the temperature dependence on susceptibilities provides the following $\chi_M T$ values (χ_M is the magnetic susceptibility per Ru^{III}Mn^{III} unit) at room temperature, 3.41 cm^3 K mol^{-1} for **1** and 3.19 cm^3 K mol^{-1} for **2**, respectively, both of which are close to the value of 3.38 cm^3 K mol^{-1} expected for one low-spin Ru(III)-centered (S = 1/2) and one high-spin Mn(III)-centered (S = 2) complexes when g = 2.00 and no exchange coupling are assumed. By lowering the temperature, the observed $\chi_M T$ values decrease smoothly and attain a minimum amount of 2.59 cm^3 K mol^{-1} at 5 K for **1** and 2.87 cm^3 K mol^{-1} at 19 K for **2**, indicating the presence of antiferromagnetic coupling between the cyanide-bridged Ru^{III}-Mn^{III} complexes. Upon further cooling, $\chi_M T$ value increases sharply to reach a maximum of 2.68 cm^3 K mol^{-1} at 2.70 K for **1** and 3.71 cm^3 K mol^{-1} at 3.40 K for **2**. When temperature of 1.90 K is applied, both $\chi_M T$ values of **1** and **2** decrease to 2.40 cm^3 K mol^{-1} for **1** and 1.20 cm^3 K mol^{-1} for **2**, respectively. Curie-Weiss fitting for **1** and **2** in the temperature range 50–300 K affords C = 3.44(1) cm^3 K mol^{-1}, θ = −1.89(3) K for **1** (Figure S2) and C =3.25(1) cm^3·K·mol^{-1}, θ = −4.41(4) K for **2** (Inset of Figure 7), respectively. The negative θ indicates a dominant antiferromagnetic (AF) coupling between spin centers. The magnetization of these compounds per [Mn^{III}Ru^{III}] unit reaches values of 3.45 Nβ mol^{-1} for **1** and 2.94 Nβ mol^{-1} for **2** at 1.90 K and 50 kOe (Figure S3 and S4, respectively), which is close to the value of 3.00 Nβ for the subtraction of one Ru^{III} and one Mn^{II} magnetic moment ($S_T = S_{Mn} - S_{Ru}$ = 3/2; $Ms = gS_T N\beta$).

According to the structures, the Ru^{III}−C≡N−Mn^{III} linkages are obviously different. An alternating ferrimagnetic chain model

$H = -J\sum_i S_{Rui}\cdot[(1+\alpha)S_{Mni} + (1-\alpha)S_{Mni+1}]$ was used[23], where the local spins are S_{Ru} and S_{Mn}, the local Zeeman factors g_{Ru} and g_{Mn}, and the couplings between nearest neighbors $J(1+\alpha)$ and $J(1-\alpha)$. The best fit between 30 and 300 K gives $g_{\mathrm{Mn}} = 2.01(1)$, $g_{\mathrm{Ru}} = 1.96(1)$, $J = -0.23(1)\ \mathrm{cm}^{-1}$, $\alpha = 0.63(1)$, and $zJ' = 0.12(3)$ ($R = 3.64\times 10^{-4}$) for **1** and $g_{\mathrm{Mn}} = 1.95(1)$, $g_{\mathrm{Ru}} = 1.99(1)$, $J = -2.67(1)\ \mathrm{cm}^{-1}$, $\alpha = -0.34(1)$, and $zJ' = -0.56(2)$ ($R = 1.16\times 10^{-4}$) for **2**, where $R = \Sigma[(\chi_{\mathrm{M}}T)_{\mathrm{obs}} - (\chi_{\mathrm{M}}T)_{\mathrm{calc}}]^2/\Sigma(\chi_{\mathrm{M}}T)_{\mathrm{obs}}{}^2$. The above mentioned result confirms that antiferromagnetic couplings between $\mathrm{Ru^{III}}$ and $\mathrm{Mn^{III}}$ ions within the chain are observed.

Magnetic properties of 3. The temperature-dependent $\chi_{\mathrm{M}}T$ for **3** is shown in Figure 8. The $\chi_{\mathrm{M}}T$ value at 300K is 1.30 $\mathrm{cm^3\cdot K\cdot mol^{-1}}$ in each $\mathrm{Ru^{III}{}_2Cu^{II}}$ unit, which is close to the theoretical value of 1.13 $\mathrm{cm^3\cdot K\cdot mol^{-1}}$ calculated from two non-coupled Ru(III) centers ($S = 1/2$) and a Cu(II) ($S = 1/2$) spin, assuming $g_{\mathrm{Ru}} = g_{\mathrm{Cu}} = 2.00$. The abrupt decrease of $\chi_{\mathrm{M}}T$ below 10 K and the negative θ values indicate a dominant antiferromagnetic (AF) coupling between $\mathrm{Ru^{III}}$ and $\mathrm{Cu^{II}}$ via C≡N bridges in **3**.[10a] in order to gain further insights into the underlying magnetic nature of **3**, the field dependence of magnetization was measured at 1.90 K (Figure 9). The magnetization increases slowly to a maximum value of 2.82 Nβ at 70 kOe, which is smaller than the expected value of 3.00 Nβ with the antiferromagnetic coupling between $\mathrm{Ru^{III}}$ and $\mathrm{Mn^{III}}$ ions. Alternating current magnetic measurements (Figure S5) show undetectable frequency-dependent χ_{M}' and χ_{M}'' signals for **3**, indicating a completely paramagnetic behavior without any magnetic ordering.

Magnetic properties of 4 and 5. The temperature-dependent magnetic susceptibilities of **4** and **5** were collected at 1 kOe in the temperature range of 1.90−300 K (Figure 9 and 10). The $\chi_{\mathrm{M}}T$ values at 300 K for **4** and **5** are 3.45 and 3.60 $\mathrm{cm^3\ K\ mol^{-1}}$, respectively, both of which are close to the spin-only value of 3.38 $\mathrm{cm^3\ K\ mol^{-1}}$ assumed for a magnetically diluted spin system (one $S_{\mathrm{Ru}} = 1/2$, $S_{\mathrm{Mn}} = 2$) with $g = 2.00$. By lowering the temperature, the $\chi_{\mathrm{M}}T$ values increase slowly by 20 K and abruptly reach a maximum of 7.40 $\mathrm{cm^3\ K\ mol^{-1}}$ at 2.20 K for **4** and 4.91 $\mathrm{cm^3\cdot K\cdot mol^{-1}}$ at 1.90 K for **5**. The continuous rise in $\chi_{\mathrm{M}}T$ at lower temperatures clearly indicates the operation of intrachain ferromagnetic couplings between Ru^{III} and Mn^{III} entities communicated by cyanide bridges. Below 2.20 K, the $\chi_M T$ value of **4** decreases sharply again and a value of 6.70 cm^3 K mol^{-1} at 1.90 K was observed. No minimum was observed in the χ_M *vs* T plots for **5**.[13] The downturn of $\chi_M T$ below 2.20 K pertains to zero-field splitting (ZFS) effect and/or interchain antiferromagnetic interactions.[12a] From the data, the Curie-Weiss fitting for **4** and **5** based on $\chi_M = C(T-\theta)$ can be carried out between 4.50 and 300 K, affording C = 3.70(1) cm^3 K mol^{-1}, θ = 1.92(8) K for **4** (Figure S6), and C = 3.49(1) cm^3 K mol^{-1}, θ = 0.14(3) K for **5** (Figure S8), respectively. The positive θ indicates a dominant ferromagnetic coupling for **4** and **5**, the behavior of which is consistent with that of other cyanide-bridged Ru–Mn compounds.[13] According to the structural data, an alternating chain model (also called the Seiden model) of quantum spins (s_i= 1/2 for Ru^{III} ion) and the classical spins (s_i= for Mn^{III} ion) based on the following spin Hamiltonian are employed.[24]

$$H = -2J\sum_{i=1}^{n}[(\hat{s}_i + \hat{s}_{i+1})\times\hat{S}_i]$$

$$x = \beta\times(-2J) = \frac{-2J}{k_B T}$$

$$\chi = \frac{0.125}{T}\times g^2\times[\frac{27}{4} + \frac{1}{1-\frac{x^2}{3}}\times(\frac{8x^2}{3} - 4x + \frac{20x^3}{9} + \frac{x^2}{2} - \frac{5x^4}{9} + \frac{25x^6}{162})]$$

Between 4.5 K and 300 K, the best least-squares fit yields g = 2.01(1), J = 0.90(1) cm^{-1}, with $R = 2.5\times 10^{-4}$ for complex **4**. The susceptibility data were fitted over 4.5 K using the same expression that gives g = 2.05(1), J = 0.37(1) cm^{-1}, with $R = 8.7\times 10^{-4}$ for complex **5**. The fitting results imply that the effect of ferromagnetic couplings between Ru^{III} and Mn^{III} ions in **4** is stronger than those in **5**.

Field-dependent magnetizations for **4** and **5** were measured from 0–70 kOe at 1.9 K (Figure 9, S9). As the intensity of applied field increases, the magnetizations continuously increase until reaching 4.10 Nβ and 3.95 Nβ at 70 kOe for **4** and **5**, respectively, which are slightly lower than the ferromagnetic result (5.00 Nβ) calculated from $M_s = g(S_{Ru} + S_{Mn})$ with g = 2.00.

To gain further insight into the underlying magnetic nature of **4**, from the dM/dH vs H plot at 1.90 K (inset of Figure 9), the critical field is estimated to be about 920 kOe. To investigate the phase transition at low temperature, ZFC and FC curves show an abrupt increase below 2.20 K with a divergence (Figure 11), suggesting the occurrence of a long-range magnetic ordering below this temperature. Furthermore, alternating current (ac) magnetic susceptibilities measurements were carried out at zero direct current (dc) field (Figure 11). The results show that only in-phase (χ_M) signals display a peak around 2.20 K, demonstrating the field-induced three-dimensional antiferromagnetic ordering below this temperature.

It is noted that the related magneto-structurally characterized analogues based on Ru^{III}–M systems were found to be either ferro- or antiferromagnetic coupling systems.[10,13,14,25,26] According to Kahn's orbital symmetry model,[20] the nature of Cu(II) and Ru(III) interaction should be ferromagnetic (J_F). The observed antiferromagnetic interaction (J_{AF}) of Cu^{II} and Ru^{III} via cyano bridges in **3** may be ascribed to the very acute Cu–N≡C angle (123.5(3)°) and long Cu···Ru distance (4.981Å). A similar antiferromagnetic interaction (J_{AF}) has also been observed in the compound $\{[Ru^{III}(Q)_2(CN)]_2(\mu\text{-}CN)_2[Cu^{II}(cyclam)]\}$.[10a] In previous studies, the ferromagnetic coupling could be universally observed in cyanide-bridged Ru(III)–Mn(III) systems.[25] For the nature of Ru^{III} and Mn^{III} interaction, it is expected that when the d_π orbitals on Ru^{III} and Mn^{III} are overlapped, antiferromagnetic interactions (J_{AF}) will emerge and vice versa. As shown in Table 6, the most complexes are in accordance with the above theoretical analysis. The magnetic behaviors of complexes **1**, **2**, **4**, and **5** appear to be slightly unusual. Especially, the bond lengths of Mn–N(cyanide) in **4** (2.292(3)–2.347(3)Å) and **5** (2.296(5)–2.322(5)Å) are in accord with those in $[Ru^{III}(salen)(CN)_2][Mn^{III}(L_2)]$[13] ($L_2$ = N,N'-(1-methylethylene) bis(2-hydroxynaphthalene-1-carbaldehydeneiminate) dianion); and the bond angles of Mn–N≡C(cyanide) (171.9(3)–176.2(4)° for **4** and 172.1(5)–172.9(7)° for **5** are remarkably larger than those in $[Ru^{III}(salen)(CN)_2][Mn^{III}(L_2)]$.[13] Magnetic investigation reveals ferromagnetic coupling in **4** and **5**. The t_{2g} orbitals of Ru^{III} and Mn^{III} overlap efficiently, resulting in the un-production of antiferromagnetic coupling and its mechanism for a magnetic exchange in the pathway of Ru^{III}-C≡N-Mn^{III} was well analyzed by Lau et al. through DFT calculations.[26] In conclusion, both the relative symmetries and relative energies of the magnetic orbitals are valuable in determining the overall magnetic coupling in bimetallic assemblies. Therefore, the full understanding of this magnetic behavior induced by energies of the magnetic orbitals deserves further investigation.

Conclusions

Five 1-D zigzag Ru^{III}–Mn^{III}/Cu^{II} chains obtained on a basis of a new paramagnetic ruthenium(III)-derived building block, *trans*-$[Ru(L)_2(CN)_2]^-$, have been synthesized and structurally characterized. Complexes **1**−**3** exhibit intrachain antiferromagnetic coupling between Ru^{III} and Mn^{III}/Cu^{II} entities through cyanide ligands, while intrachain ferromagnetic coupling between Ru^{III} and Mn^{III} through cyanide ligands can be observed for complexes **4** and **5**. It is noteworthy that complex **4** shows interesting metamagnetic behaviors with a critical field of about 920 Oe at 1.9 K. Furthermore, magneto-structural correlation for some typical cyano-bridged heterobimetallic Ru^{III}−Mn^{III}/Cu^{II} compounds has been discussed in this work. It can be assumed that the relative symmetries and their corresponding magnetic orbital energies are valuable in determining the overall magnetic coupling in bimetallic assemblies. On the basis of the above mentioned results, the present work shows that the type of $[Ru(L)_2(CN)_2]^-$ building block is useful for the construction of low-dimensional 3d-4d magnetic materials.

Acknowledgments

This work was supported by the Major State Basic Research Development Program (2013CB922101), the National Natural Science Foundation of China (51173075), and the Natural Science Foundation of Jiangsu Province (BK20130054). We also thank Dr. Tian-Wei Wang for the experimental assistance on magnetic measurements.

Supporting Information

Additional structures, spectroscopic data, magnetic characterization data, and X-ray crystallographic files in CIF formats for **1–5**. This material is available free of charge via the Internet at http://www.rsc.org.

References

1. (a) S. Wang, J. L. Zuo, H. C. Zhou, H. J. Choi, Y. X. Ke, J. R. Long and X. Z. You, *Angew. Chem., Int. Ed.*, 2004, **43**, 5940-5943; (b) K. Qian, X. C. Huang, C. Zhou, X. Z. You, X. Y. Wang and K. R. Dunbar, *J. Am. Chem. Soc.*, 2013, **135**, 13302-13305; (c) K. S. Pedersen, J. Bendix and R. Clerac, *Chem. Commun.*, 2014, **50**, 4396-4415; (d) N. Hoshino, F. Iijima, G. N. Newton, N. Yoshida, T. Shiga, H. Nojiri, A. Nakao, R. Kumai, Y. Murakami and H. Oshio, *Nat. Chem.*, 2012, **4**, 921-926;(e) D. P. Dong, T. Liu, S. Kanegawa, S. Kang, O. Sato, C. He and C. Y. Duan, *Angew. Chem., Int. Ed.*, 2012, **51**, 5119-5123;(f) K. J. Cho, D. W. Ryu, H. Y. Kwak, J. W. Lee, W. R. Lee, K. S. Lim, E. K. Koh, Y. W. Kwon and C. S. Hong, *Chem. Commun.*, 2012, **48**, 7404-7406.
2. (a) X. Y. Wang, C. Avendano and K. R. Dunbar, *Chem. Soc. Rev.*, 2011, **40**, 3213-3238; (b) R. Lescouëzec, L. M. Toma, J. Vaissermann, M. Verdaguer, F. S. Delgado, C. Ruiz-Pérez, F. Lloret and M. Julve, *Coord. Chem. Rev.*, 2005, **249**, 2691-2729; (c) L. M. Baraldo, P. Forlano, A. R. Parise, L. D. Slep and J. A. Olabe, *Coord. Chem. Rev.*, 2001, **219**, 881-921.
3. S. Wang, X. H. Ding, Y. H. Li and W. Huang, *Coord. Chem. Rev.*, 2012, **256**, 439-464.
4. (a) X. Feng, J. Liu, T. D. Harris, S. Hill and J. R. Long, *J. Am. Chem. Soc.*, 2012, **134**, 7521-7529.
5. J. M. Zadrozny, D. E. Freedman, D. M. Jenkins, T. D. Harris, A. T. Iavarone, C. Mathoniere, R. Clerac and J. R. Long, *Inorg. Chem.*, 2010, **49**, 8886-8896.
6. (a) T. S. Venkatakrishnan, S. Sahoo, N. Brefuel, C. Duhayon, C. Paulsen, A. L. Barra, S. Ramasesha and J. P. Sutter, *J. Am. Chem. Soc.*, 2010, **132**, 6047-6056; (b) D. Pinkowicz, R. Podgajny, R. Pelka, W. Nitek, M. Balanda, M. Makarewicz, M. Czapla, J. Zukrowski, C. Kapusta, D. Zajac and B. Sieklucka, *Dalton Trans.*,

2009, 7771-7777; (c) B. Yan, H. Zhou and A. Lachgar, *Inorg. Chem.*, 2003, **42**, 8818-8822.

7. (a) M. Perrier, J. Long, F. A. Paz, Y. Guari and J. Larionova, *Inorg. Chem.*, 2012, **51**, 6425-6427; (b) S. Ren, S.-L. Ma, G.-F. Xu, B. Gu, Y. Ma, Q.-L. Wang and D.-Z. Liao, *Inorg. Chem. Commun.*, 2011, **14**, 1124-1127; (c) R. Podgajny, S. Choraży, W. Nitek, A. Budziak, M. Rams, C. J. Gómez-García, M. Oszajca, W. Łasocha and B. Sieklucka, *Cryst. Growth Des.*, 2011, **11**, 3866-3876; (d) J. Long, E. Chelebaeva, J. Larionova, Y. Guari, R. A. Ferreira, L. D. Carlos, F. A. Almeida Paz, A. Trifonov and C. Guerin, *Inorg. Chem.*, 2011, **50**, 9924-9926.
8. (a) D. Visinescu, R. Jeon Ie, A. M. Madalan, M. G. Alexandru, B. Jurca, C. Mathoniere, R. Clerac and M. Andruh, *Dalton Trans.*, 2012, **41**, 13578-13581; (b) M. G. Alexandru, D. Visinescu, A. M. Madalan, F. Lloret, M. Julve and M. Andruh, *Inorg. Chem.*, 2012, **51**, 4906-4908; (c) D. Li, L. Zheng, Y. Zhang, J. Huang, S. Gao and W. Tang, *Inorg. Chem.*, 2003, **42**, 6123-6129.
9. (a) E. V. Peresypkina, D. G. Samsonenko and K. E. Vostrikova, *J. Solid State Chem.*, 2015, **224**, 107-114; (b) D. G. Samsonenko, C. Paulsen, E. Lhotel, V. S. Mironov and K. E. Vostrikova, *Inorg. Chem.*, 2014, **53**, 10217-10231; (c) M. R. Saber and K. R. Dunbar, *Chem. Commun.*, 2014, **50**, 2177-2179.
10. (a) J. Xiang, L. H. Jia, B. W. Wang, S. M. Yiu, S. M. Peng, W. Y. Wong, S. Gao and T. C. Lau, *Dalton Trans.*, 2013, **42**, 3876-3887; (b) W. F. Yeung, W. L. Man, W. T. Wong, T. C. Lau and S. Gao, *Angew. Chem., Int. Ed.*, 2001, **40**, 3031-3033.
11. W. F. Yeung, P. H. Lau, T. C. Lau, H. Y. Wei, H. L. Sun, S. Gao, Z. D. Chen and W. T. Wong, *Inorg. Chem.*, 2005, **44**, 6579-6590.
12. G. Marinescu, C. Maxim, R. Clérac, and M. Andruh, *Inorg. Chem.*, 2015, **51**, 5621-5623.
13. J. H. Yoon, H. S. Yoo, H. C. Kim, S. W. Yoon, B. J. Suh and C. S. Hong, *Inorg. Chem.*, 2009, **48**, 816-818.
14. (a) J. Ru, F. Gao, M. X. Yao, T. Wu and J. L. Zuo, *Dalton Trans.*, 2014, **43**, 18047-18055; (b) J. Ru, F. Gao, T. Wu, M. X. Yao, Y. Z. Li and J. L. Zuo, *Dalton*

Trans., 2014, **43**, 933-936; (c) L.Cui, F.F. Zhu, C. F. Leong, J. Ru, F. Gao, D. M. D'Alessandro and J. L. Zuo, *Sci.China Chem.*, 2015, **58**, 650-657.

15. (a) A. G. Smith, P. A. Tasker, D. White, *J. Coord. Chem. Rev.,* 2003, **241**, 61−85; (b) P. Tasker, V. Gasperov, *Macrocyclic Chem*., 2005, 365−382; (c) J. Szymanowski, Hydroxyoximes and Copper Hydrometallurgy; CRC Press: Boca Raton, FL, 1993.
16. A. Kumar Das, S. -M. Peng and S. Bhattacharya, *J. Chem. Soc., Dalton Trans.*, 2000, 181–184
17. (a) M. X. Yao, Q. Zheng, X. M. Cai, Y. Z. Li, Y. Song and J. L. Zuo, *Inorg. Chem.*, 2012, **51**, 2140-2149; (b) M. X. Yao, Q. Zheng, F. Gao, Y. Z. Li, and J. L. Zuo, *Sci.China Chem.*, 2012, **55**, 1022-1030.
18. C. F. Wang, D. P. Li, X. Chen, X. M. Li, Y. Z. Li, J. L. Zuo and X. Z. You, *Chem. Commun.*, 2009, 6940-6942.
19. W. H. Leung and C. M. Che, *Inorg. Chem.*, 1989, **28**, 4619-4622.
20. *SAINT-Plus*, *version 6.02*, Bruker Analytical X-ray System, Madison, WI, 1999.
21. G. M. Sheldrick, *SADABS an empirical absorption correctionprogram*, Bruker Analytical X-ray Systems, Madison, WI, 1996.
22. G. M. Sheldrick, *SHELXTL-97*, Universität of Göttingen, Göttingen, Germany, 1997.
23. O. Kahn, *Molecular Magnetism*, VCH: Weinhem, Germany, 1993.
24. J. Seiden, *J. Phys. Lett.*, 1983, **44**, L947-L952.
25. D. P. Zhang, L. -F. Zhang, Y. T. Chen, H. L. Wang, Z. -H. Ni,W.Wernsdorferc, J. Z. Jiang, *Chem. Commun.*, 2010, **46**, 3550-3552.
26. J.-F. Guo, X.-T. Wang, B. -W. Wang, G.-C. Xu, S. Gao, L. Szeto, W.-T. Wong, W.-Y. Wong, T.-C. Lau, *Chem. Eur. J.,* 2010, **16**, 3524.

Table 1. Summary of crystallographic data for complexes **1**–**5**.

	1	**2**	**3**	**4**	**5**
formula	$C_{68}H_{60}Mn_2N_{12}O_8Ru_2$	$C_{38}H_{34}MnN_6O_4Ru$	$C_{48}H_{48}CuN_{12}O_4Ru_2$	$C_{43}H_{36}MnN_6O_4Ru$	$C_{46}H_{34}MnN_6O_4Ru$
fw	1485.30	794.72	1122.66	856.79	890.80
crystal system	Triclinic	Triclinic	Triclinic	Triclinic	Triclinic
space group	$P\bar{1}$	$P\bar{1}$	$P\bar{1}$	$P\bar{1}$	$P\bar{1}$
a, Å	12.573(2)	11.3228(8)	9.9611(13)	11.2322(11)	11.680(3)
b, Å	15.090(3)	13.2197(10)	12.0243(16)	12.9655(13)	13.560(3)
c, Å	21.612(4)	14.3410(11)	12.4374(17)	17.3258(18)	17.386(4)
α, deg	100.154(3)	79.9650(10)	103.509(2)	84.393(2)	82.361(4)
β, deg	103.996(3)	85.0240(10)	102.368(2)	81.625(2)	78.858(4)
γ, deg	94.967(3)	81.5080(10)	94.169(2)	71.103(2)	67.126(3)
V, Å^3	3880.5	2086.5(3)	1403.0(3)	2358.3(4)	2484.2(10)
Z	2	2	1	2	2
ρ_{calcd},gcm^{-3}	1.268	1.262	1.324	1.204	1.188
T / K	296(2)	293(2)	293(2)	296(2)	293(2)
μ, mm^{-1}	0.754	0.706	0.955	0.630	0.600
F(000)	1504	810	569	874	906
data/restraints/parameters	13506/0/836	7306/0/470	6244/24/365	8285/0/490	8712/0/499
GOF (F^2)	0.932	1.179	1.061	1.143	1.103
R_1^a,wR_2^b(I>2σ(I))	0.0567, 0.1475	0.0591, 0.1392	0.0425, 0.1484	0.0345, 0.1060	0.0655,0.1723
R_1^a, wR_2^b(all data)	0.0824, 0.1610	0.0671, 0.1429	0.0459, 0.1541	0.0461, 0.1119	0.0904,0.1825

$R_1^a = \Sigma||F_o| - |F_c||/\Sigma F_o|$. $wR_2^b = [\Sigma w(F_o^2 - F_c^2)^2/\Sigma w(F_o^2)^2]^{1/2}$

Table 2. Selected bond lengths (Å) and angles (°) for complex **1**.

C(9)-Ru(1)	2.057(5)	C(26)-Ru(2)	2.067(5)
O(5)-Ru(2)	1.969(3)	Ru(1)-C(9)#1	2.057(5)
N(1)-Ru(1)	2.040(4)	N(6)-Ru(2)	2.037(4)
N(7)-Ru(2)	2.049(4)	Ru(1)-N(1)#1	2.040(4)
Ru(1)-O(1)#1	1.986(3)	Mn(1)-O(2)	1.902(4)
Mn(1)-O(3)	1.883(4)	Mn(1)-N(4)	1.989(4)
Mn(1)-N(3)	1.975(4)	Mn(1)-N(5)	2.298(4)
Mn(1)-N(2)	2.248(4)	Mn(2)-O(6)	1.879(3)
Mn(2)-N(8)	2.288(4)	N(8)-C(43)-Ru(2)	178.9(5)
N(2)-C(9)-Ru(1)	177.8(5)	N(5)-C(26)-Ru(2)	173.9(5)
C(9)-N(2)-Mn(1)	163.6(4)	C(26)-N(5)-Mn(1)	158.2(5)
C(43)-N(8)-Mn(2)	161.8(4)	C(60)-N(11)-Mn(2)	159.9(5)

Symmetry transformations used to generate equivalent atoms:#1: −x+2,−y+2,−z+2; #2:−x+1,−y+1,−z.

Table 3. Selected bond lengths (Å) and angles (°) for complex **2**.

C(37)–Ru(1)	2.062(6)	C(38)-Ru(2)	2.066(6)
Mn(1)-N(1)	1.994(5)	Mn(1)-N(2)	2.011(5)
Mn(1)-O(1)	1.864(4)	Mn(1)-O(2)	1.873(4)
Mn(1)-N(5)	2.396(5)	Mn(1)-N(6)	2.315(5)
N(3)-Ru(2)	2.045(4)	N(4)-Ru(1)	2.021(5)
O(3)-Ru(2)	2.005(3)	O(4)-Ru(1)	1.982(4)
N(5)-C(37)-Ru(1)	174.5(5)	N(6)-C(38)-Ru(2)	175.4(5)
C(37)-N(5)-Mn(1)	150.1(5)	C(38)-N(6)-Mn(1)	153.3(4)

Table 4. Selected bond lengths (Å) and angles (°) for complex **3**.

N(5)-Cu(1)	2.051(3)	N(6)-Cu(1)	2.002(4)
Cu(1)-N(6')#2	2.002(4)	Cu(1)-N(6)#2	2.002(4)
Cu(1)-N(5')#2	2.051(3)	Cu(1)-N(5)#2	2.051(3)
Cu(1)-N(4)	2.411(4)	Cu(1)-N(4)#2	2.411(4)
N(1)-Ru(2)	2.048(4)	N(3)-Ru(1)	2.046(3)

O(1)-Ru(2)	1.988(3)	O(2)-Ru(1)	1.982(3)
N(4)-C(18)-Ru(1)	177.9(4)	C(18)-N(4)-Cu(1)	123.5(3)

Symmetry transformations used to generate equivalent atoms:#1: −x,−y+2,−z+1; #2: −x+1, −y+2, −z+1; #3: −x+1, −y+1, −z+1.

Table 5. Selected bond lengths (Å) and angles (°) for complex **4**.

Ru(1)-O(1)#1	1.9904(17)	Ru(1)-O(1)	1.9904(17)
Ru(1)-N(1)	2.036(2)	Ru(1)-N(1)	2.036(2)
Ru(1)-C(9)#1	2.077(3)	Ru(1)-C(9)	2.077(3)
Ru(2)-C(35)	2.072(3)	Ru(2)-C(35)#2	2.072(3)
Ru(2)-N(6)	2.037(2)	Ru(2)-N(6)#2	2.037(2)
Ru(2)-O(4)	1.988(2)	Ru(2)-O(4)#2	1.988(2)
Mn(1)-O(3)	1.8847(19)	Mn(1)-O(2)	1.8978(19)
Mn(1)-N(3)	1.971(2)	Mn(1)-N(4)	1.974(2)
Mn(1)-N(5)	2.292(3)	Mn(1)-N(2)	2.347(3)
N(2)-C(9)-Ru(1)	178.4(3)	C(35)-N(5)-Mn(1)	171.9(3)
N(5)-C(35)-Ru(2)	175.3(3)	C(9)-N(2)-Mn(1)	176.2(3)

Symmetry transformations used to generate equivalent atoms:#1 −x+2, −y, −z; #2 −x+1,−y+1,−z+1.

Table 6. Selected bond lengths (Å) and angles (°) for complex **5**.

Mn(1)-O(2)	1.889(4)	Mn(1)-O(3)	1.909(4)
Mn(1)-N(5)	1.941(6)	Mn(1)-N(4)	1.974(5)
Mn(1)-N(3)	2.296(5)	Mn(1)-N(6)	2.322(5)
Ru(1)-O(1)#1	1.998(4)	Ru(1)-O(1)	1.998(4)
Ru(1)-N(1)	2.050(4)	Ru(1)-N(1)#1	2.050(4)
Ru(1)-C(44)	2.101(5)	Ru(1)-C(44)#1	2.101(5)
Ru(2)-O(4)#2	1.977(4)	Ru(2)-O(4)	1.978(4)
Ru(2)-C(45)#2	2.067(6)	Ru(2)-N(7)	2.007(6)
N(3)-C(44)-Ru(1)	174.0(5)	N(6)-C(45)-Ru(2)	177.6(7)
C(44)-N(3)-Mn(1)	172.1(5)	C(45)-N(6)-Mn(1)	172.9(7)

Symmetry transformations used to generate equivalent atoms: #1 −x,−y+1,−z+2 #2 −x+1,−y,−z+1.

Table 7. Structural and magnetic parameters for related cyano-bridged Ru^{III}-Mn^{III} complexes.

Complexes	$d_{Mn\text{-}N}$/Å	Ru-C-N(deg)	Mn-N-C(deg)	J_{exp}/cm^{-1}	ref
$Ru(salen)CN_2[Mn(L_1)]$	2.292-2.307	169.9-170.6	143.1-144.3	1.34	13
$\{[Ru(Q)_2](\mu\text{-}CN)_2[Mn(salcy)]\}_n$	2.286	175.7	154.2-149.6	−0.75	10a
$[\{Mn(5,5'\text{-}Me_2salen)\}_2\{Ru(acac)_2(CN)_2\}][Ru(acac)_2(CN)_2]\cdot 2CH_3OH$	2.165	178.3	168.1	0.87,0.24	26
$\{[Ru(acac)_2(CN)_2]\ [Mn(TPP)]\}\ \{[Ph_3(PhCH_2)P]PF_6\}_2CH_3OH$	2.251	177.5	152.3	3.25	25
$\{[Ru(acac)_2(CN)_2]\ [Mn(TPP)]\}\{[Ph_3(PhCH_2)P]ClO_4\}_2CH_3OH$	2.250	177.7	153.0	3.43	25
$[Ru(salen)(CN)_2Mn(R,R\text{-}salcy)]_n$	2.325-2.354	174.2-175.4	156.4-154.3	−0.40, −1.32	14a
$[Ru(salen)(CN)_2Mn(R,R\text{-}salphen)]_n$	2.331-2.349	168.9-178.0	158.7-174.8	−1.25, −1.87	14a
1	2.248-2.298	177.8	158.2-163.6	−0.37, −0.08	This paper
2	2.315-2.396	174.5	150.1-153.3	−3.26, −1.43	This paper
4	2.292-2.347	178.4	171.9-176.2	0.90	This paper
5	2.296-2.322	174.0	172.9-172.1	0.37	This paper

H_2TPP = *meso*-tetra(4-phenyl)-porphyrin.

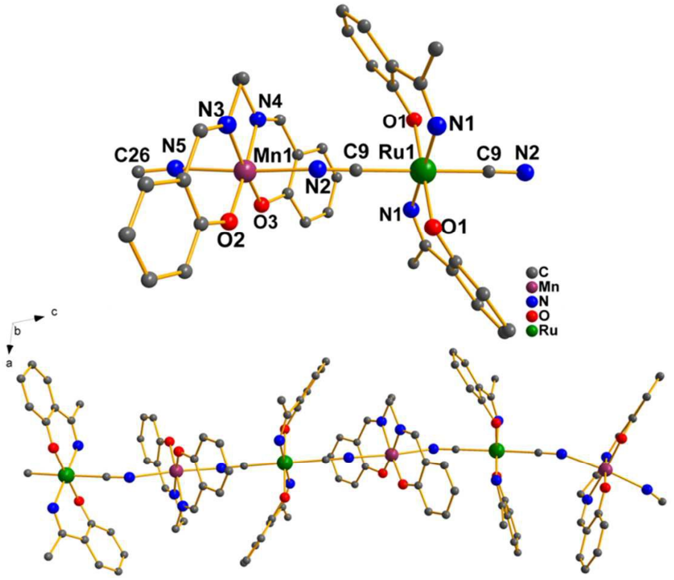

Figure 1. Asymmetric unit (top) and one-dimensional chain structure (bottom) of complex **1**. Hydrogen atoms are omitted for clarity.

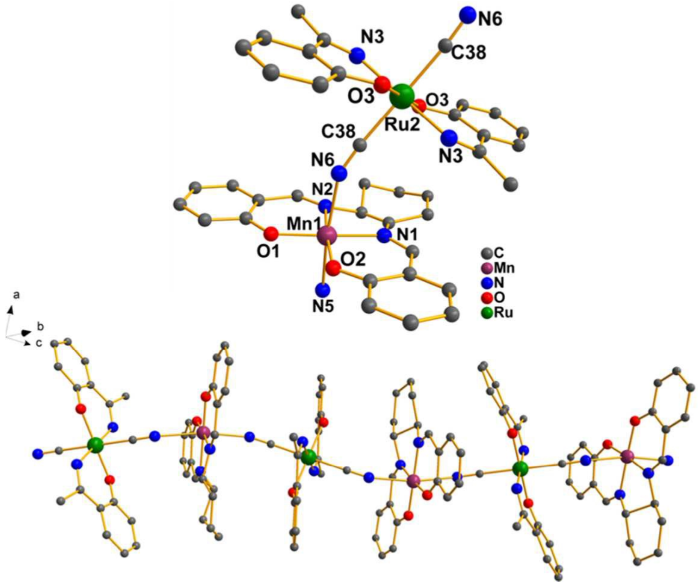

Figure 2. Asymmetric unit (top) and one-dimensional chain structure (bottom) of complex **2**. Hydrogen atoms are omitted for clarity.

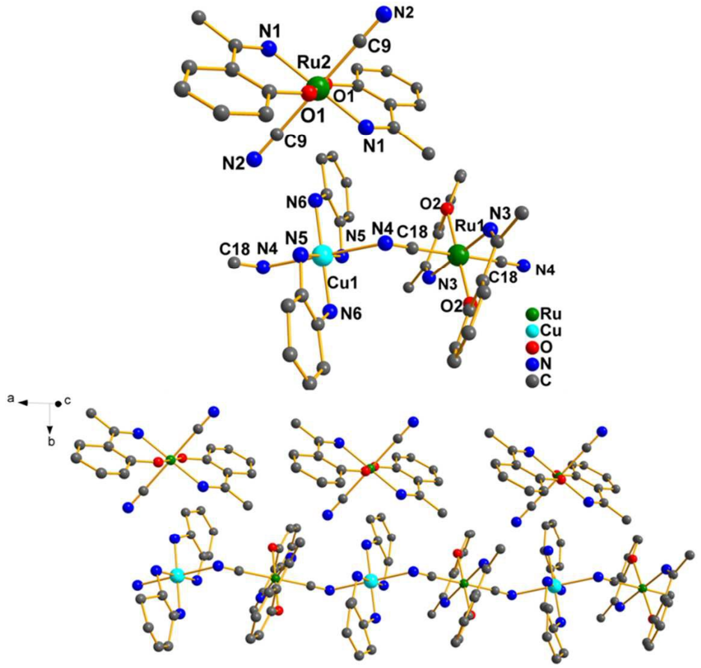

Figure 3. Asymmetric cationic unit (top) and one-dimensional cationic chain structure (bottom) of complex **3**. Hydrogen atoms are omitted for clarity.

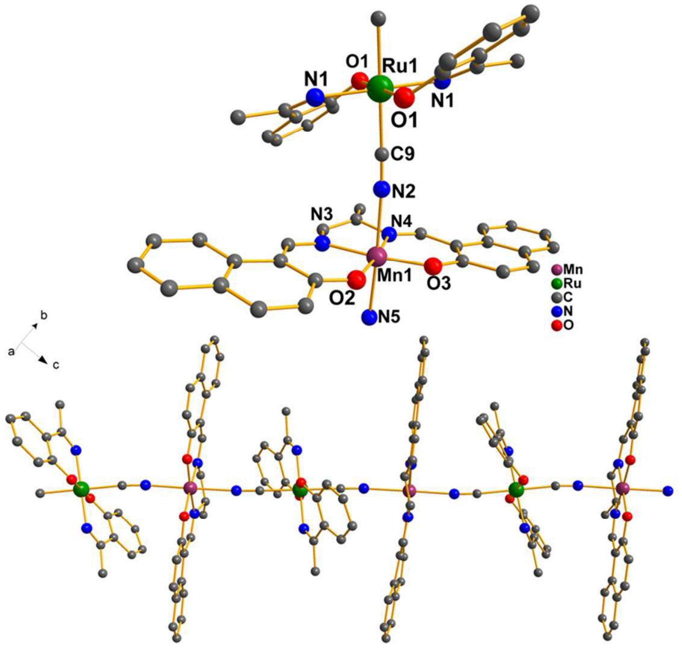

Figure 4. Asymmetric unit (top) and one-dimensional chain structure (bottom) of complex **4**. Hydrogen atoms are omitted for clarity.

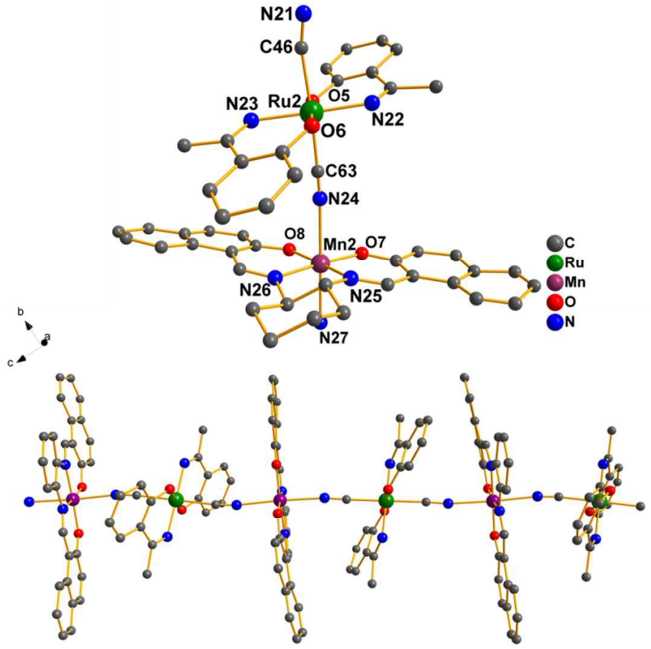

Figure 5. Asymmetric unit (top) and one-dimensional chain structure (bottom) of complex **5**. Hydrogen atoms are omitted for clarity.

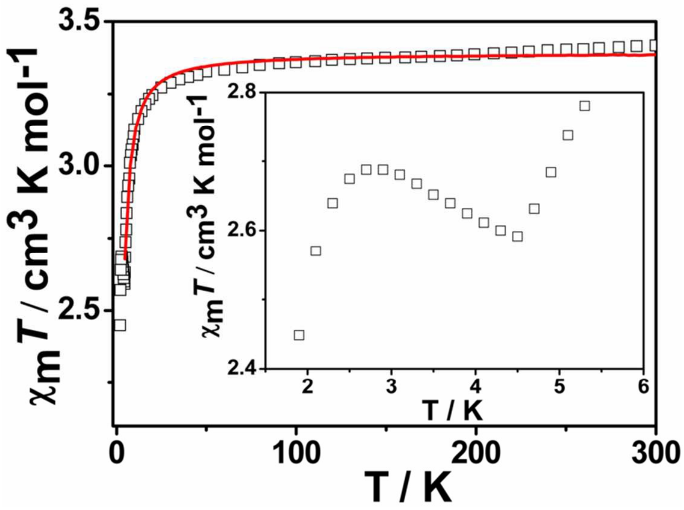

Figure 6. Temperature dependence of $\chi_M T$ (□) at 1 kOe and (inset) $\chi_M T$ for complex **1** at 1.9 - 6 K.

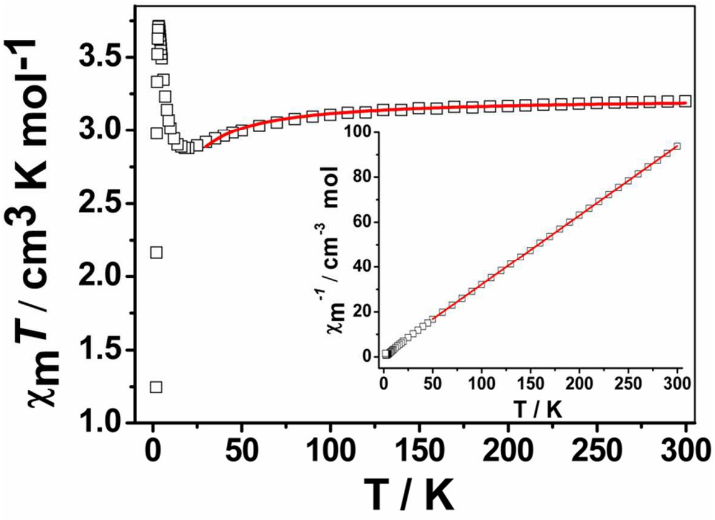

Figure 7. Temperature dependence of χ_MT (□) and (Inset) $1/\chi_M$(□) for complex **2** at 1 kOe.

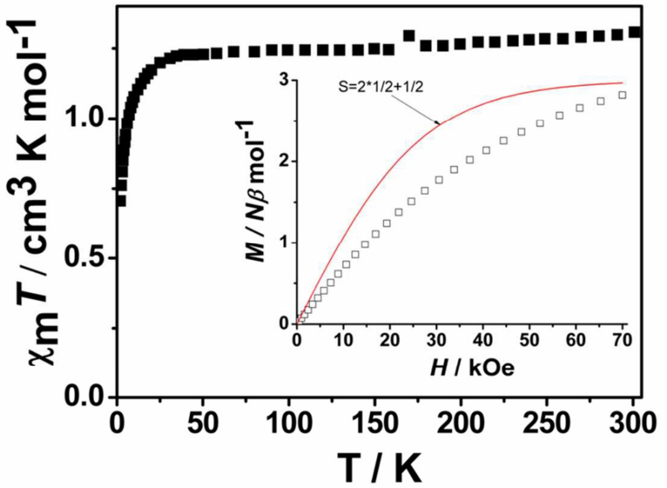

Figure 8. Temperature dependence of the χ_MT product for **3** at 1 kOe. (Inset) Field dependence of the magnetization for **3**, the lines represent the Brillouin function that correspond to $S = 1/2+2$ with $g = 2.0$.

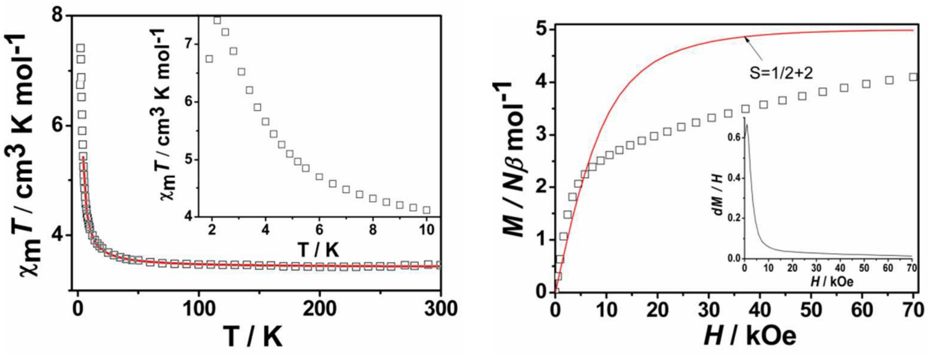

Figure 9. Left: Temperature dependence of $\chi_M T$ (□) at 1 kOe and (Inset) $\chi_M T$ for complex **4** at 1.9 - 10 K. Right: Field dependence of the magnetization for **4**, the red line represent the Brillouin function that correspond to $S = 1/2+2$ with $g = 2.0$. (Inset) dM/dH vs H plot at 1.9 K.

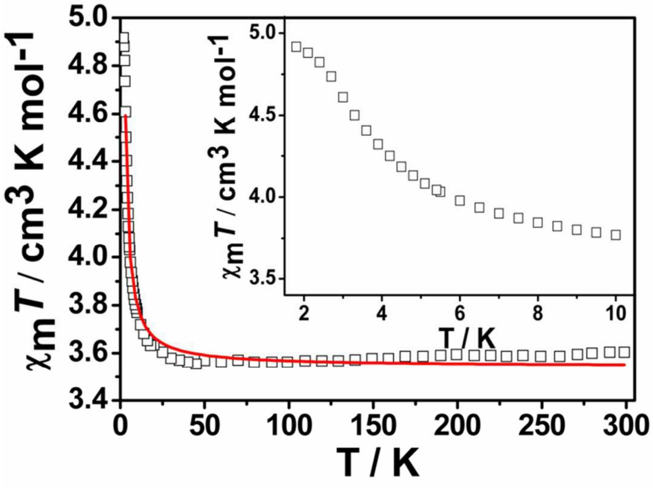

Figure 10. Temperature dependence of $\chi_M T$ (□) 1 kOe and (Inset) $\chi_M T$ for complex **5** at 1.9 – 10 K.

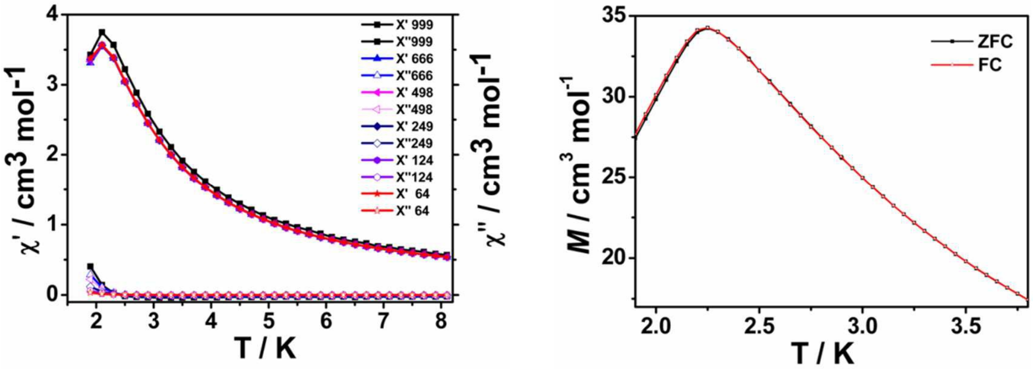

Figure 11. Left: Temperature dependence of the in-phase χ' (top) and out-of-phase χ'' (bottom) at different frequencies in 2 Oe ac field oscillating at 1-999 Hz with zero applied dc field for **4**. Right: Temperature dependence of the magnetization for **4** at 10 Oe.